Supporting Information for:

A simple copper(II) dppy-based receptor for sensing of L-Cysteine and L-Histidine in aqueous acetonitrile medium

Dipankar Das,[a] Aritra Roy,[b,c] Sourav Sutradhar,[a] Felipe Fantuzzi*,[d] and Biswa Nath Ghosh*,[a]

[a.] *Department of Chemistry, National Institute of Technology Silchar, Silchar-788010, Assam, India. Tel: +91-8018123682, E-mail: bnghosh@che.nits.ac.in.*
[b.] *Department of Chemistry, Pondicherry University, Pondicherry 605014, India.*
[c.] *Current Address: Department of Chemical and Energy Engineering, London South Bank University, 103 Borough Road, London SE1 0AA, UK.*
[d.] *School of Chemistry and Forensic Science, University of Kent, Park Wood Rd, Canterbury CT2 7NH, UK. E-mail: f.fantuzzi@kent.ac.uk.*

Table of contents

1 – Synthesis of L

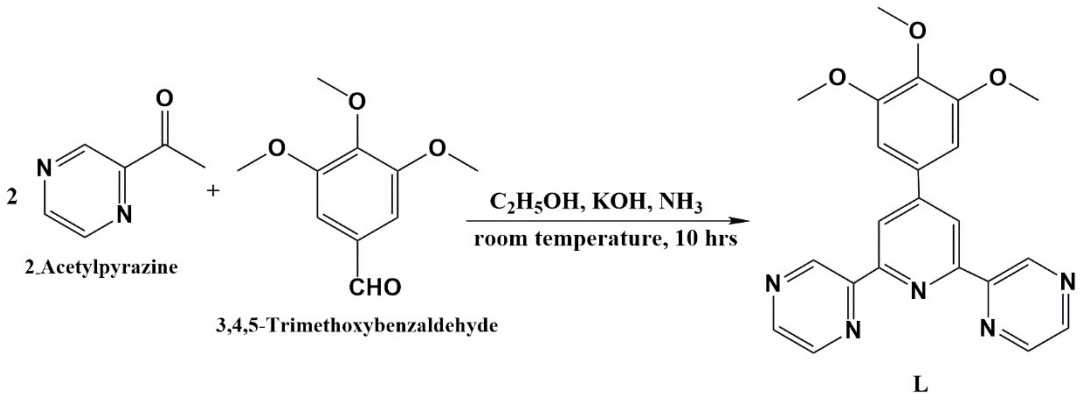

Scheme S1 Schematic Representation of Synthesis of **L**

2 – NMR data

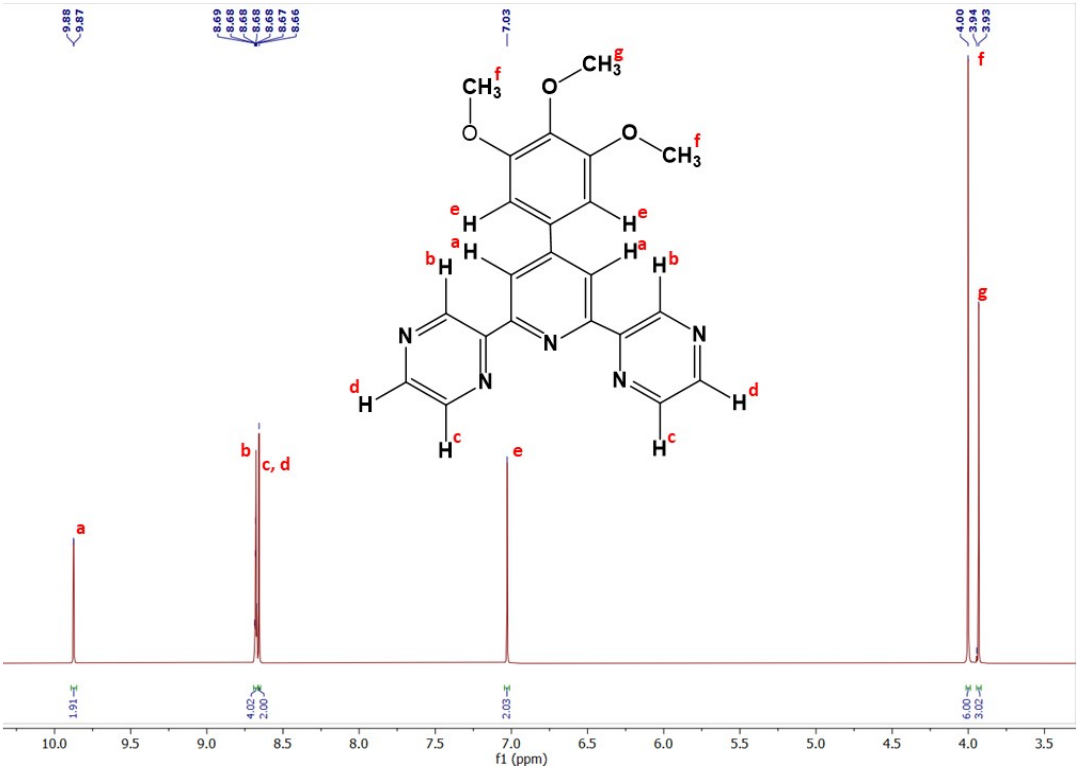

Figure S1 500 MHz ^{1}H NMR spectrum of **L** in $CDCl_3$.

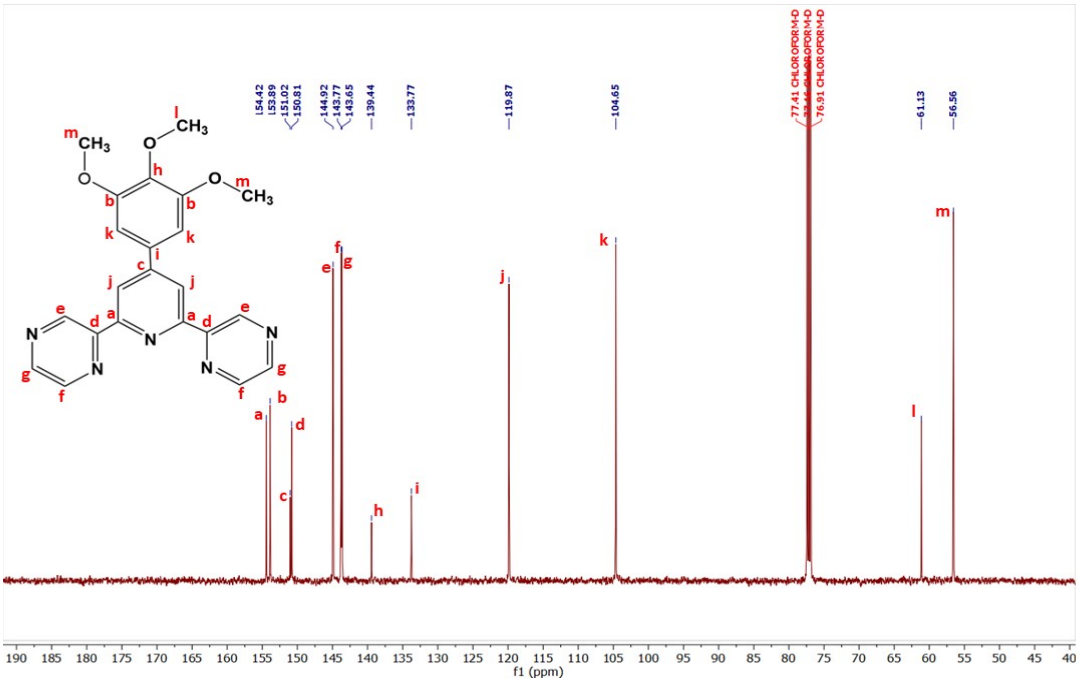

Figure S2 125 MHz ^{13}C NMR spectrum of **L** in $CDCl_3$.

3 – ESI-HRMS, FT-IR and EPR data

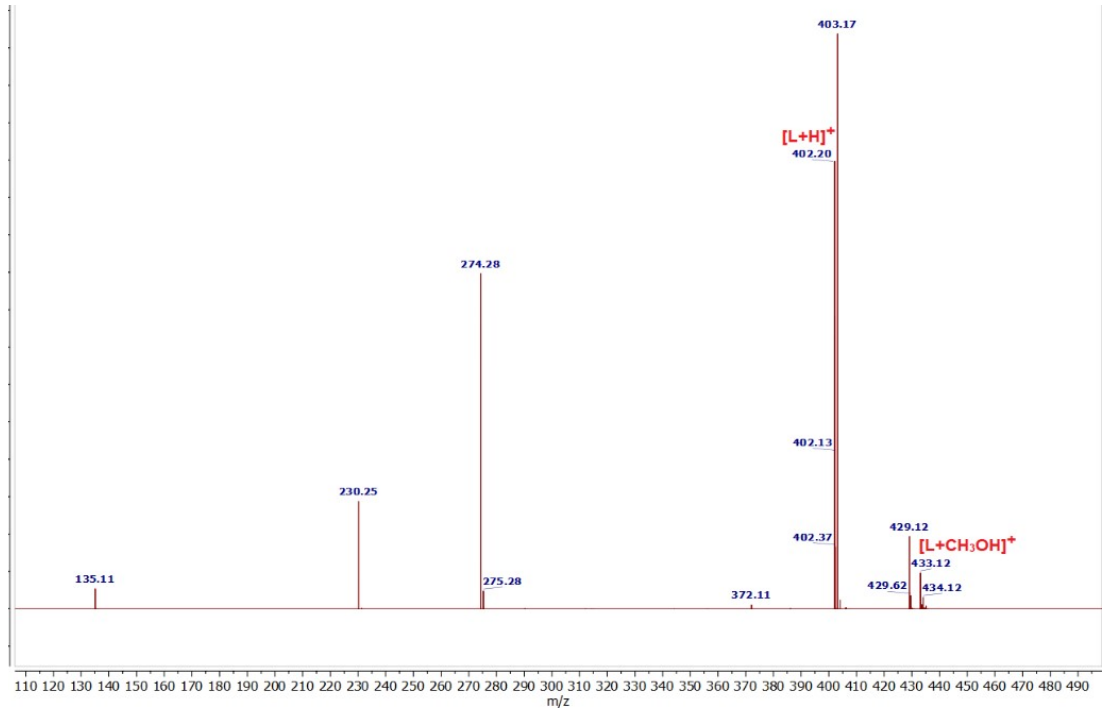

Figure S3 ESI-HRMS spectrum of **L**.

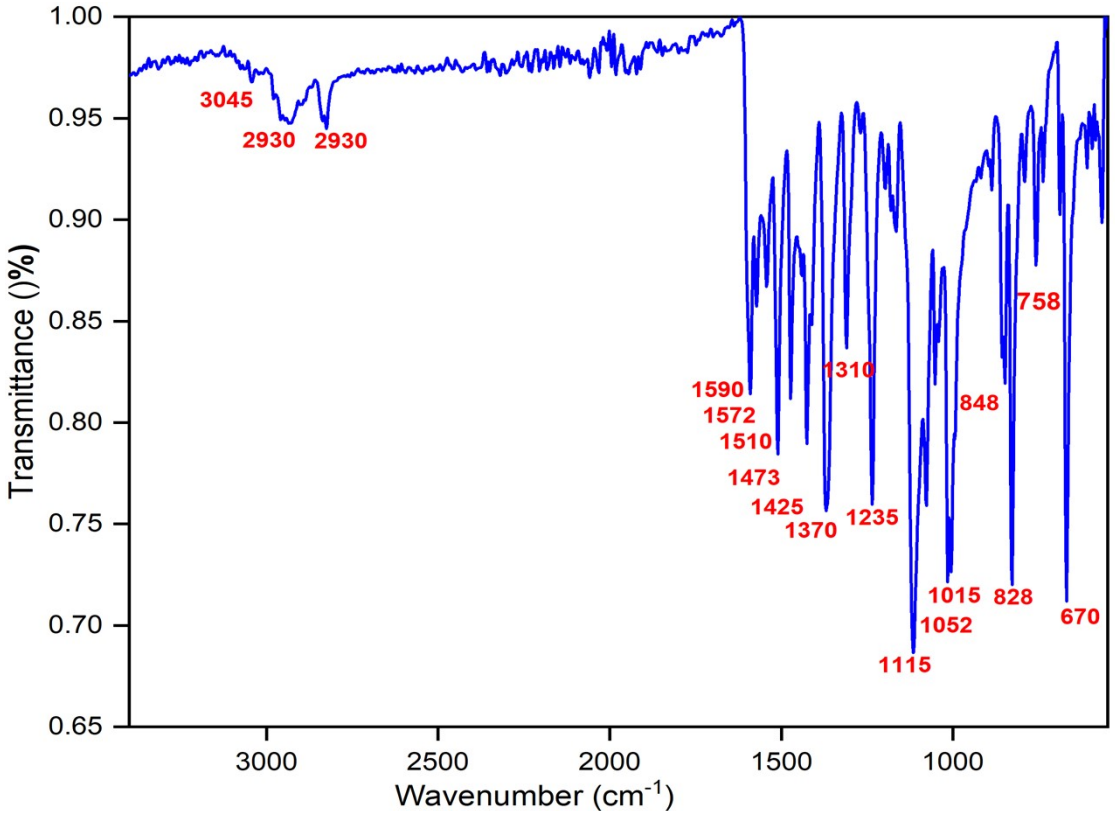

Figure S4 FT-IR spectrum of **L**.

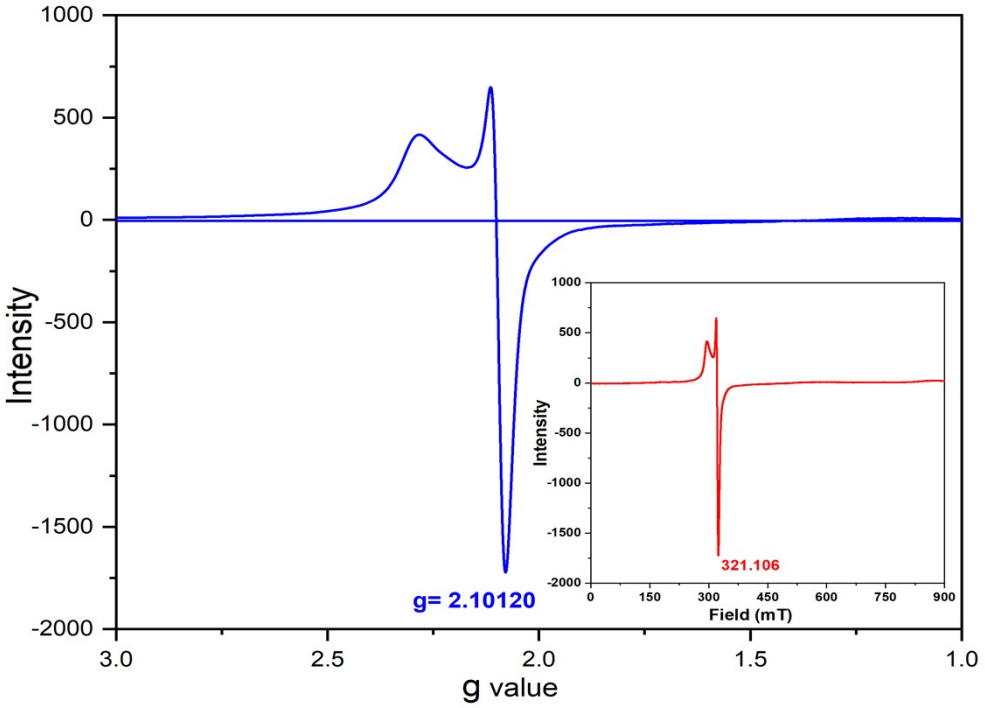

Figure S5 X-band EPR spectra of **$CuCl_2L$**.

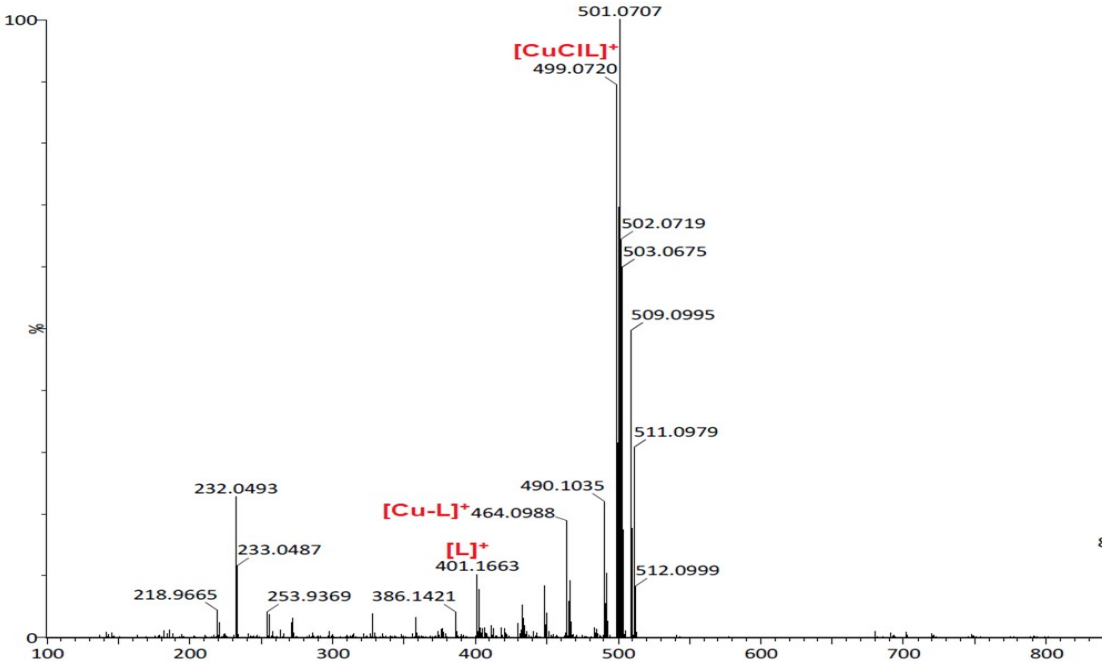

Figure S6 ESI-HRMS spectrum of **$CuCl_2L$**.

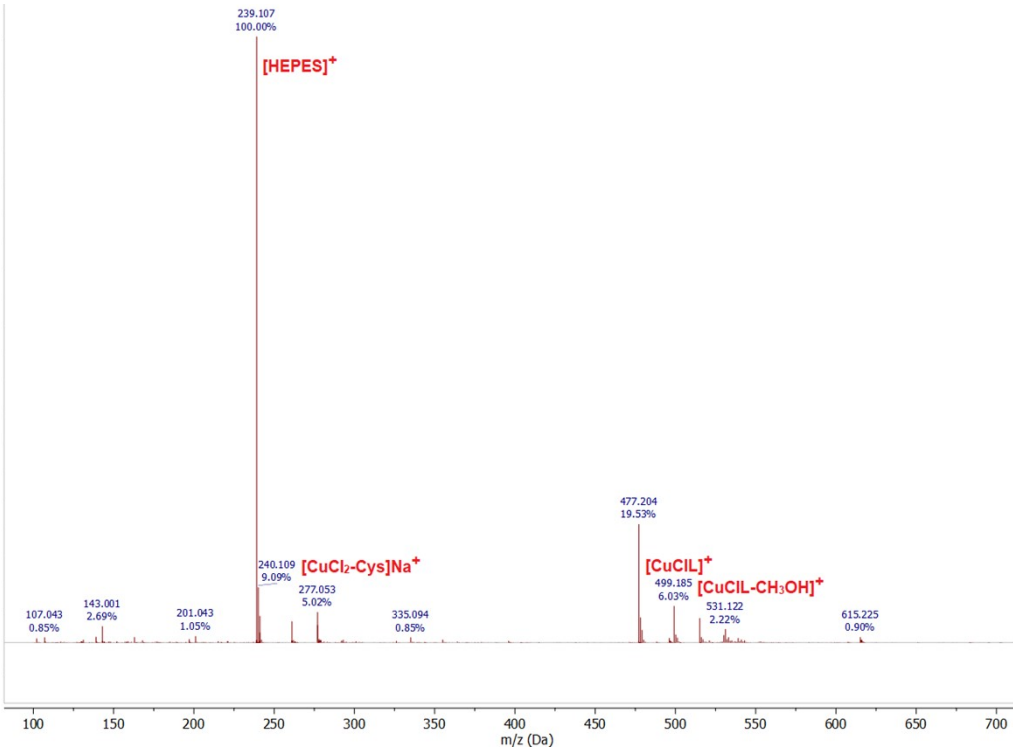

Figure S7 ESI-HRMS spectrum of *in-situ* prepared **$CuCl_2L$** (30 µM, 2 mL) with Cys (1 mM, 60 µL) in aqueous acetonitrile (4:1 *v/v,* 10 mM HEPES, pH 7.4).

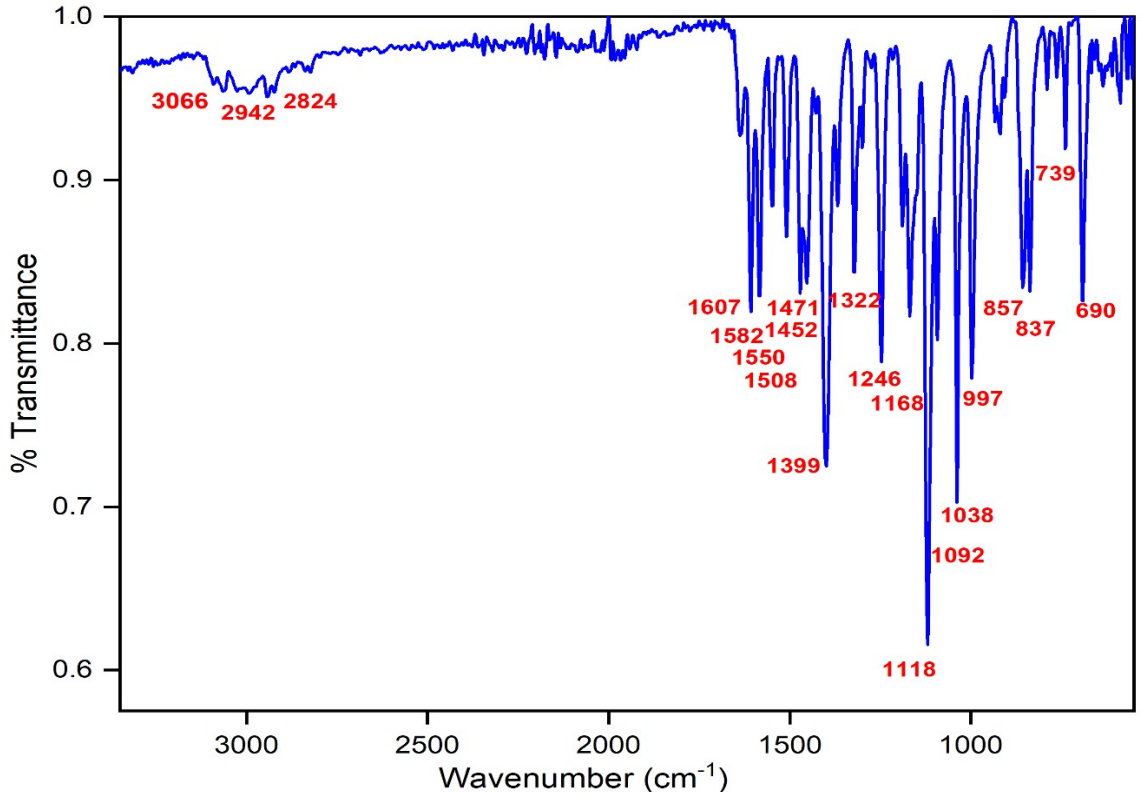

Figure S8 FT-IR spectrum of **$CuCl_2L$**.

4 – UV-Visible absorption spectra

An UV-Visible absorption spectral titration was carried out by gradually adding aqueous copper chloride solution (1 mM, 5-45 µL) to an acetonitrile solution of **L** (200 µM, 400 µL) in water (1.6 mL, 10 mM HEPES, pH 7.4) and calculated the stability constant for formation of **$CuCl_2$L** using the Benesi–Hildebrand (B-H) equation[1] given below:

$$\frac{1}{A - Ao} = \frac{1}{A_{Max} - A} + \frac{1}{k \times (A_{Max} - A)} \times \frac{1}{[CuCl_2]}$$

The stability constant (*k*) for the **$CuCl_2$L** complex formation by the reaction between ligand **L** and copper chloride was found to be 7.285×10^4 M^{-1}.

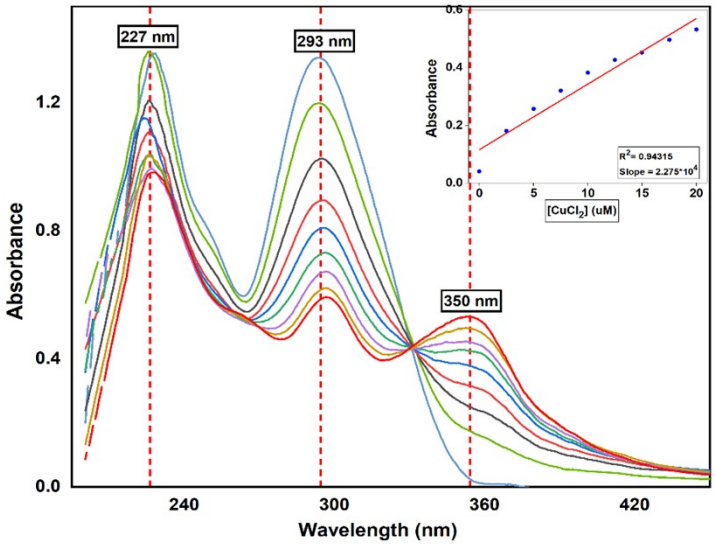

Figure S9 Absorption spectra of acetonitrile solution of **L** (200 µM, 400 µL) in water (1.6 mL, 10 mM HEPES, pH 7.4) upon gradual addition of aqueous copper chloride solution (1 mM, 5-45 µL) (Inset: Absorption intensity variation of 350 nm absorption band).

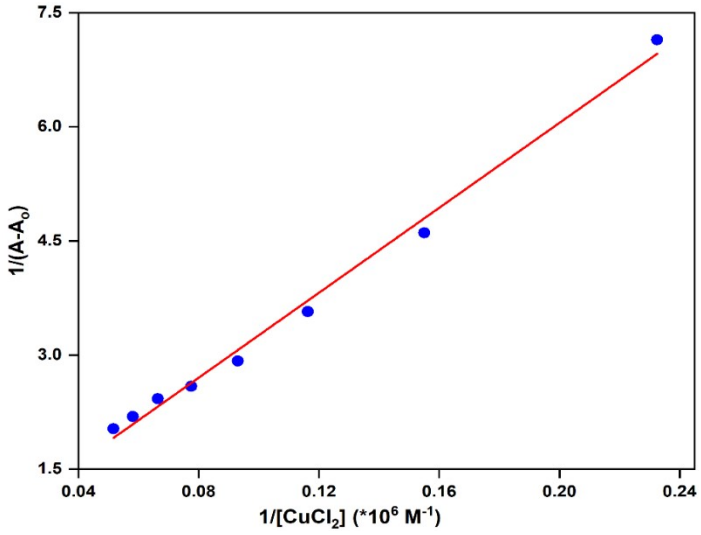

Figure S10: B-H Plot for the calculation of the stability constant of **$CuCl_2L$**

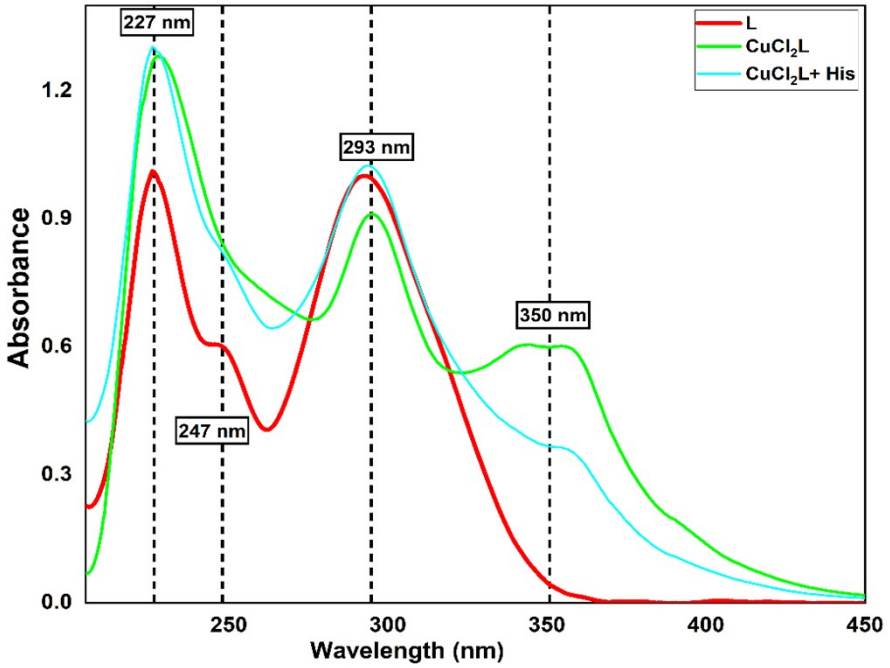

Figure S11 Absorption spectra of the *in-situ* prepared **$CuCl_2L$** (30 µM, 2 mL) upon addition of His (1 mM, 60µL) in aqueous acetonitrile (4:1 *v/v,* 10 mM HEPES, pH 7.4).

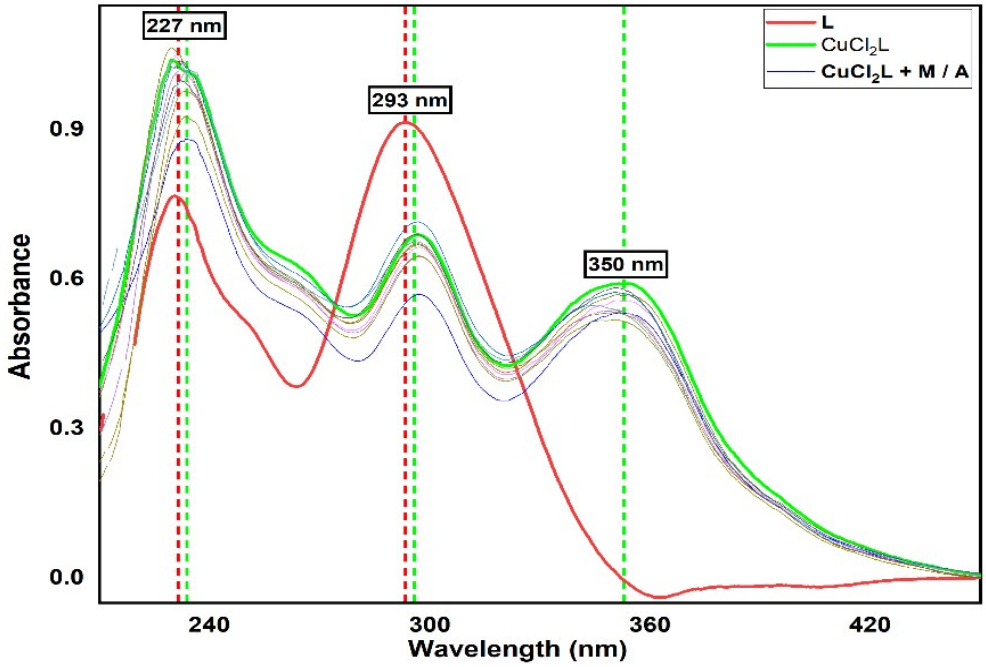

Figure S12 Absorption spectra of the *in-situ* prepared **$CuCl_2L$** (30 µM, 2 mL) upon addition of one equivalent different metals (nitrate salts of Mg^{2+}, Ca^{2+}, Sr^{2+}, Ba^{2+}, chloride salts of Mn^{2+}, Co^{2+}, Ni^{2+}, Cu^{2+}, Zn^{2+}, and Cd^{2+},1 mM, 60 µL), and ten equivalents different anions (Sodium

salts of PPi, HPO_4^{2-}, N_3^-, F^-, I^-, OH^-, $CH_3CO_2^-$, SO_4^{2-}, SO_3^{2-}, $S_2O_3^{2-}$, Cl^-, HCO_3^-, $H_2PO_4^-$, CO_3^{2-}, Br^-, SO_3^{2-}, NO_3^-, 10 mM, 60 µL) in aqueous acetonitrile (4:1 *v/v,* 10 mM HEPES, pH 7.4).

Effect of *p*H variation on *in-situ* prepared $CuCl_2L$ receptor, and its Cys and His detection studies

We have carried out effect of *p*H variation studies on *in-situ* prepared **$CuCl_2L$** receptor, and its Cys and His detection abilities at various *p*H (*p*H range 4-10) with the help of UV-Visible absorption spectral study. The results of these studies indicated that **$CuCl_2L$** receptor stable enough at 4 ≤ *p*H ≤ 9 to carry out sensing studies. It was also found that the receptor complex hydrolysed at *p*H < 4 or *p*H > 9. The **$CuCl_2L$** receptor was most effective for Cys (one equivalent) sensing study for 4 ≤ *p*H ≤ 9, while 6.5 ≤ *p*H ≤ 9 is most effective for His (one equivalent) sensing study. At pH ≤ 6.0, binding sites of His moiety got protonated, resulting in decrease in the binding affinity of histidine towards **$CuCl_2L$** receptor.

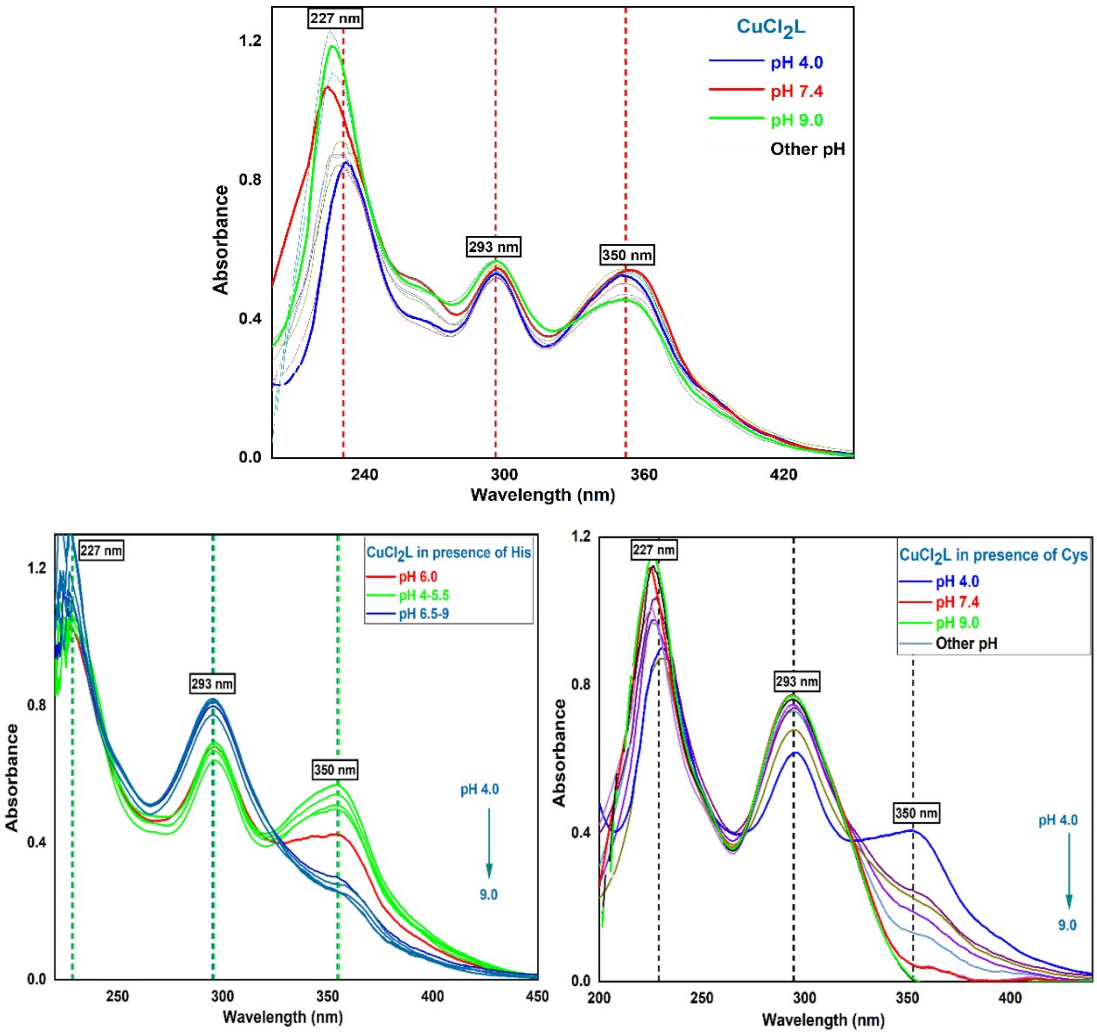

Figure S13 UV-Visible absorption spectra of **a)** *in-situ* prepared **$CuCl_2L$** (30 µM, 2 mL) and **b)** *in-situ* prepared **$CuCl_2L$** (30 µM, 2 mL) with Cys (1 eq., 1 mM, 60 µL) in aqueous acetonitrile (4:1 *v*/*v,* 10 mM HEPES, 4 ≤ *p*H ≤ 9). **c**) *in-situ* prepared **$CuCl_2L$** (30 µM, 2 mL) with Cys (1 eq., 1 mM, 60 µL) in aqueous acetonitrile (4:1 *v*/*v,* 10 mM HEPES, 6.5 ≤ *p*H ≤ 9).

5 – Limit of detection (LOD) calculation

The limit of detection (LOD) is calculated using a simple relation between Signal-to-Noise ratio (3 or 3.3), the standard deviation of the blank solution (σ) and slope of the calibration line (S). The LOD may be expressed as:

$$LOD = \frac{3.3 \times \sigma}{S}$$

Where, **σ** was calculated by measuring absorption spectra of "n" number of **$CuCl_2L$** receptor in aqueous acetonitrile (4:1 *v*/*v,* 10 mM HEPES buffer, pH 7.4) as blank sample (n=10 times) and then calculated the standard deviation of these responses (0.00425).

6 – Computational data

Complete computational description of the Cu:Cys and Cu:His complexes

Regarding the metal site, we examined both the bare, open-shell Cu(II) ion and the neutral, open-shell $CuCl_2$ moiety in our calculations. Consequently, we focused our investigations on the structure of [CuCys] and $[CuCysCl_2]^{2-}$ complexes. Whenever appropriate, we compared our [CuCys] results with those of $[CuCys]^{2+}$ by Belcastro and co-workers.[90] Regarding His, we only considered the R–CH(NH_2)–COO^- anionic state. As a result, we thoroughly examined the characteristics of $[CuHisCl_2]^-$ and $[Cu(His)_2]$ complexes. Figures S14(**B**-**C**) show the optimised structures of the most stable [CuCys] and $[CuCysCl_2]^{2-}$ complexes. The first number indicates the free energy (ΔG_0) of each structure relative to that of the most stable conformer (values in kcal mol^{-1}). Subsequently, the following numbers represent the free energies of reaction used to characterise the stability of the complexes. They are labelled as follows: binding free energy (ΔG_1 for $[CuCysCl_2]^{2-}$; $\Delta G_{1'}$, for [CuCys]), and ligand exchange free energy (ΔG_2, for $[CuCysCl_2]^{2-}$; $\Delta G_{2'}$, for [CuCys]). These values are associated with the following equations:

$CuCl_2 + Cys^{2-} \rightarrow [CuCysCl_2]^{2-}$, ΔG_1 (1.1)

$CuCl_2 + Cys^{2-} \rightarrow [CuCys] + 2Cl^-$, $\Delta G_{1'}$ (1.2)

$CuCl_2L + Cys^{2-} \rightarrow [CuCysCl_2]^{2-} + L$, ΔG_2 (2.1)

$CuCl_2L + Cys^{2-} \rightarrow [CuCys] + L + 2Cl^-$, $\Delta G_{2'}$ (2.2)

All ΔG_i values are calculated in solution and at 298 K, with concentration corrections also considered. It is possible to see that, contrary to $[CuCys]^{2+}$,[90] where the lowest energy conformation presents a bidentate *O,S*-coordination, the global minimum structure of $[CuCysCl_2]^{2-}$ features a more favourable *N,S*-coordination. In contrast, neutral [CuCys] prefers a tridentate *N,O,S*-coordination. These modes are more favourable than the conformers containing an *O,S*-coordination by ΔG_0 = 3.0 kcal mol^{-1} and 5.8 kcal mol^{-1}, respectively, with the *N,O,S*-coordination of [CuCys] just slightly more favourable than the *N,S*-coordination (ΔG_0 = +2.2 kcal mol^{-1}). For $[CuCysCl_2]^{2-}$, while the *N,O*-coordination is less stable than the *N,S*-coordination by ΔG_0 = +8.3 kcal mol^{-1}, the worst bidentate binding mode occurs through the two oxygen atoms (ΔG_0 = +20.1 kcal mol^{-1}). The ΔG_0 values of the [CuCys] complexes follow a similar trend, with the *N,O*- and *O,O*-coordination modes less favourable than the *N,S* one by +18.1 kcal mol^{-1} and +26.4 kcal mol^{-1}. In $[CuCysCl_2]^{2-}$, the *N,O,S* coordination mode

is less stable than the *N,S* mode by ΔG_0 = +15.6 kcal mol^{-1}, highlighting that the Cl ligands disfavour the increase of the denticity of the amino acid by charge repulsion.

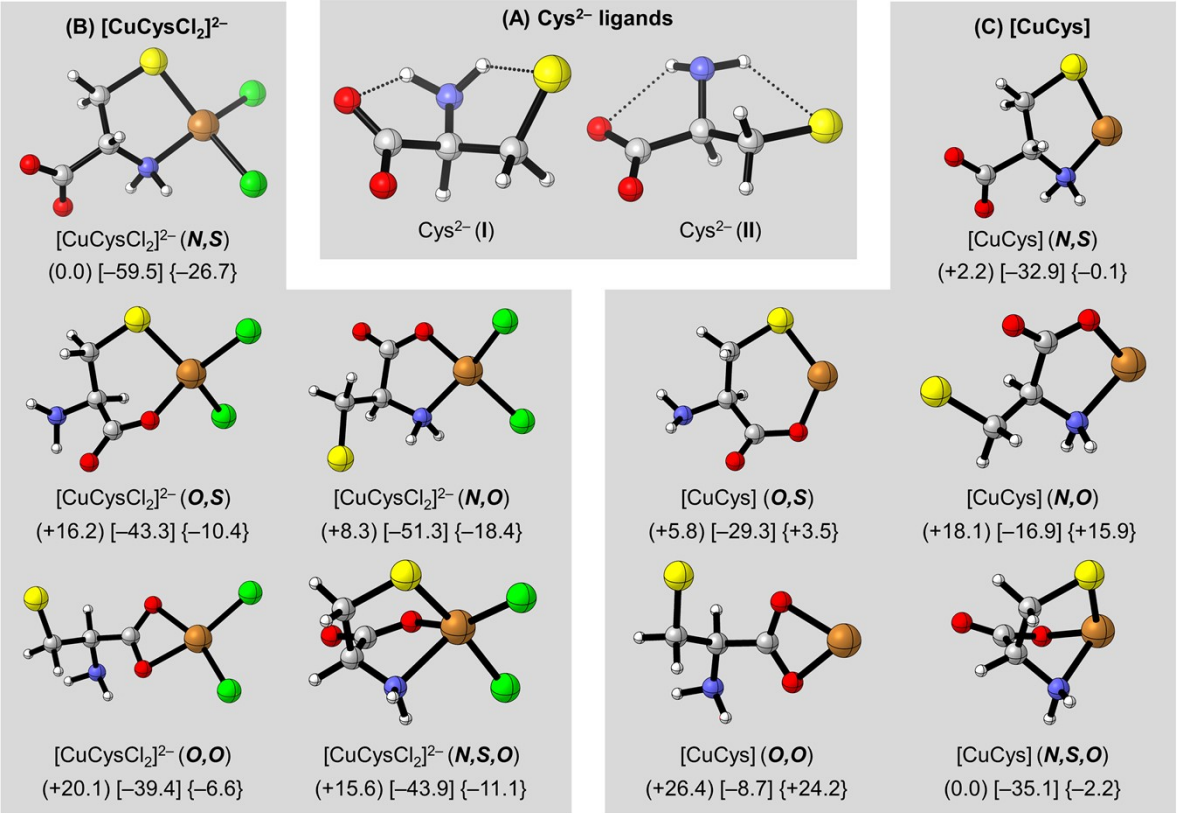

Figure S14 Most stable structures of **(A)** Cys^{2-}, **(B)** $[CuCysCl_2]^{2-}$ and **(C)** [CuCys] at the SMD/PBE0-D3(BJ)/bs2 level of theory. The numbers below the 3D plots are ΔG_0, ΔG_1 (or $\Delta G_{1'}$), and ΔG_2 (or $\Delta G_{2'}$), expressed in kcal mol^{-1} (for more details, see text). Geometries were optimised at the PBE0-D3(BJ)/bs1 level. Gray: carbon; white: hydrogen; red: oxygen; blue: nitrogen; green: chlorine; yellow: sulphur; orange: copper.

Next, we turn our attention to the binding and ligand exchange free energy values. The *N,S*-coordination of $[CuCysCl_2]^{2-}$ features the most negative binding free energy value amongst the systems investigated here, with ΔG_1 = –59.5 kcal mol^{-1}. Combining this value with that of the formation of **$CuCl_2L$**, we find that the ligand exchange free energy of this $[CuCysCl_2]^{2-}$ conformer is ΔG_2 = –26.7 kcal mol^{-1}, also by far the most negative value across the systems analysed. It is noteworthy that, amongst the computed [CuCys] systems, only the *N,S*- ($\Delta G_{2'}$ = –0.1 kcal mol^{-1}) and the *N,O,S*-coordination mode ($\Delta G_{2'}$ = –2.2 kcal mol^{-1}) complexes exhibit exergonic behaviour concerning ligand exchange coupled with Cl^- elimination. In contrast, the computed ΔG_2 values for $[CuCysCl_2]^{2-}$ complexes are consistently

exergonic. These findings strongly indicate that the Cl groups remain indeed bound to Cu following coordination with Cys. This aligns well with the experimental data, which also supports the presence of such coordination.

With respect to histidine, the following equations were used to describe the stability of its copper complexes:

$CuCl_2 + His^- \rightarrow [CuHisCl_2]^-$, ΔG_3 (3)

$CuCl_2 + 2\ His^- \rightarrow [Cu(His)_2] + 2Cl^-$, ΔG_4 (4)

$CuCl_2L + His^- \rightarrow [CuHisCl_2]^- + L$, ΔG_5 (5)

$CuCl_2L + 2\ His^- \rightarrow [Cu(His)_2] + L + 2Cl^-$, ΔG_6 (6)

where ΔG_3 and ΔG_4 are related to binding free energies and ΔG_5 and ΔG_6 to the ligand exchange free energies, the even equations coupled with Cl^- elimination. The most stable $[CuHisCl_2]^-$ species features histidine working as a bidentate ligand, binding $CuCl_2$ through the NH_2 and the deprotonated nitrogen of the imidazole ring (Figure S15, left). While the binding free energy of His in this complex, as indicated by its ΔG_3 value of –44.4 kcal mol^{-1}, is indeed more negative than the binding energy of **$CuCl_2L$** (–32.9 kcal mol^{-1}), it is significantly less negative compared to the corresponding value for $[CuCysCl_2]^{2-}$ (–59.4 kcal mol^{-1}). Consequently, ΔG_5 is exergonic by merely –11.5 kcal mol^{-1}, less than half of the corresponding ΔG_2 value of $[CuCysCl_2]^{2-}$ (–26.7 kcal mol^{-1}). In contrast, our stability analysis revealed that $[Cu(His)_2]$ is preferably formed. Indeed, the ΔG_6 value of $[Cu(His)_2]$ is –21.8 kcal mol^{-1}, slightly less exergonic than the ΔG_2 value of $[CuCysCl_2]^{2-}$. Hence, unlike Cys, our findings suggest that His exhibits a preference for forming complexes with the bare Cu(II) ion rather than $CuCl_2$. The most stable structure of $[Cu(His)_2]$ features a mixed configuration (Figure S15, right), where one His works as a tridentate ligand with *N,N,O*-coordination, and the other as a bidentate ligand through the amino and carboxyl groups (*N,O*-coordination). Our computational findings substantiate the observed differences in the stoichiometric ratio between copper cysteine and histidine complexes. Furthermore, they provide compelling evidence that the selectivity of **$CuCl_2L$** in amino acid sensing is attributed to the exceptionally stable coordination modes formed between $CuCl_2$ and the cysteine and histidine residues.

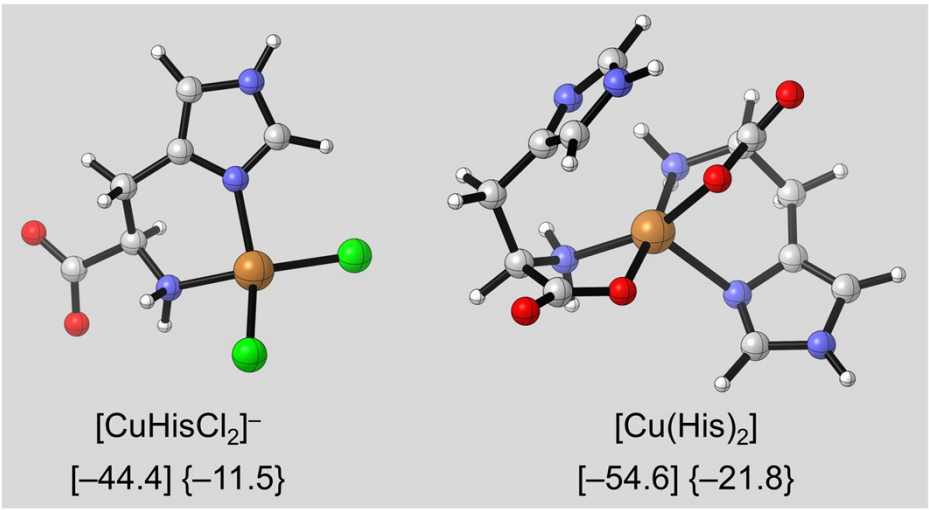

Figure S15 Most stable structures of $[CuHisCl_2]^-$ and $[Cu(His)_2]$ at the SMD/PBE0-D3(BJ)/bs2 level of theory. The numbers below the 3D plots are ΔG_3 and ΔG_5 for $[CuHisCl_2]^-$ and ΔG_4 and ΔG_6 for $[Cu(His)_2]$, respectively. Geometries were optimised at the PBE0-D3(BJ)/bs1 level. For low-lying isomers, see Figures S17. And S18. Gray: carbon; white: hydrogen; red: oxygen; blue: nitrogen; green: chlorine; orange: copper.

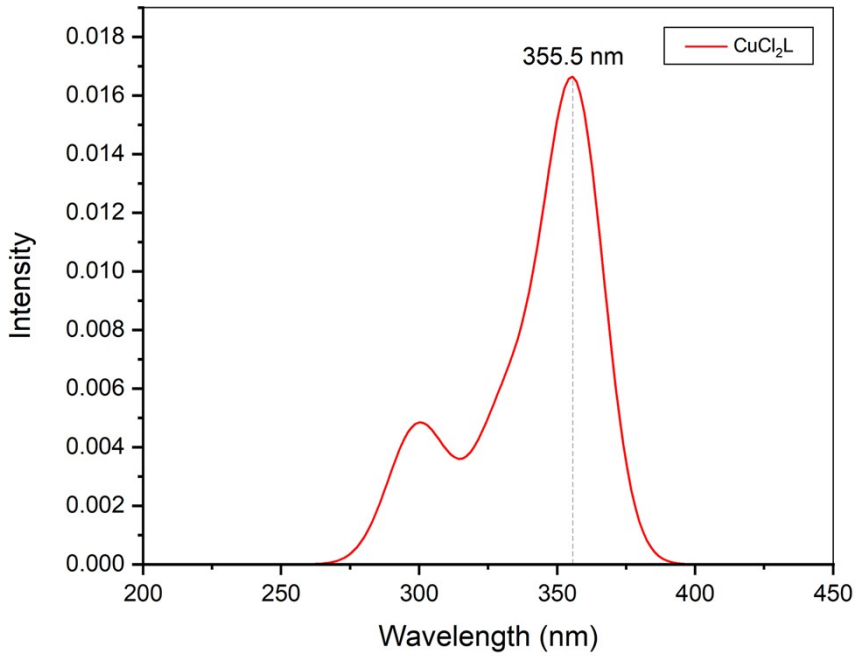

Figure S16 TD-DFT computed UV-Vis spectrum of **$CuCl_2$L** at the SMD/ωB97X-D/bs2 level of theory.

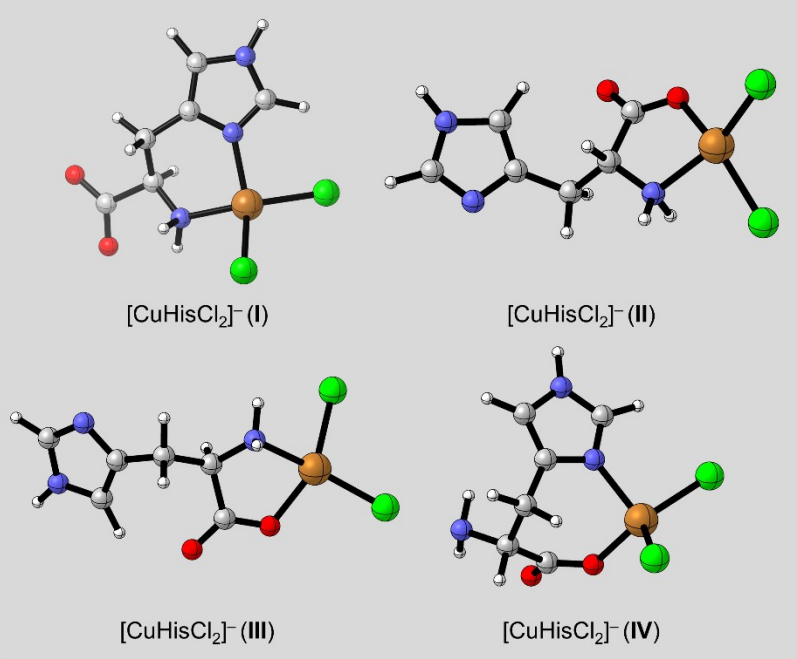

Figure S17 Free energies of all $[CuHisCl_2]^{2-}$ structures investigated herein at the SMD/PBE0-D3(BJ)/bs2 level of theory. Geometries were optimised at the PBE0-D3(BJ)/bs1 level. Gray: carbon; white: hydrogen; red: oxygen; blue: nitrogen; orange: copper.

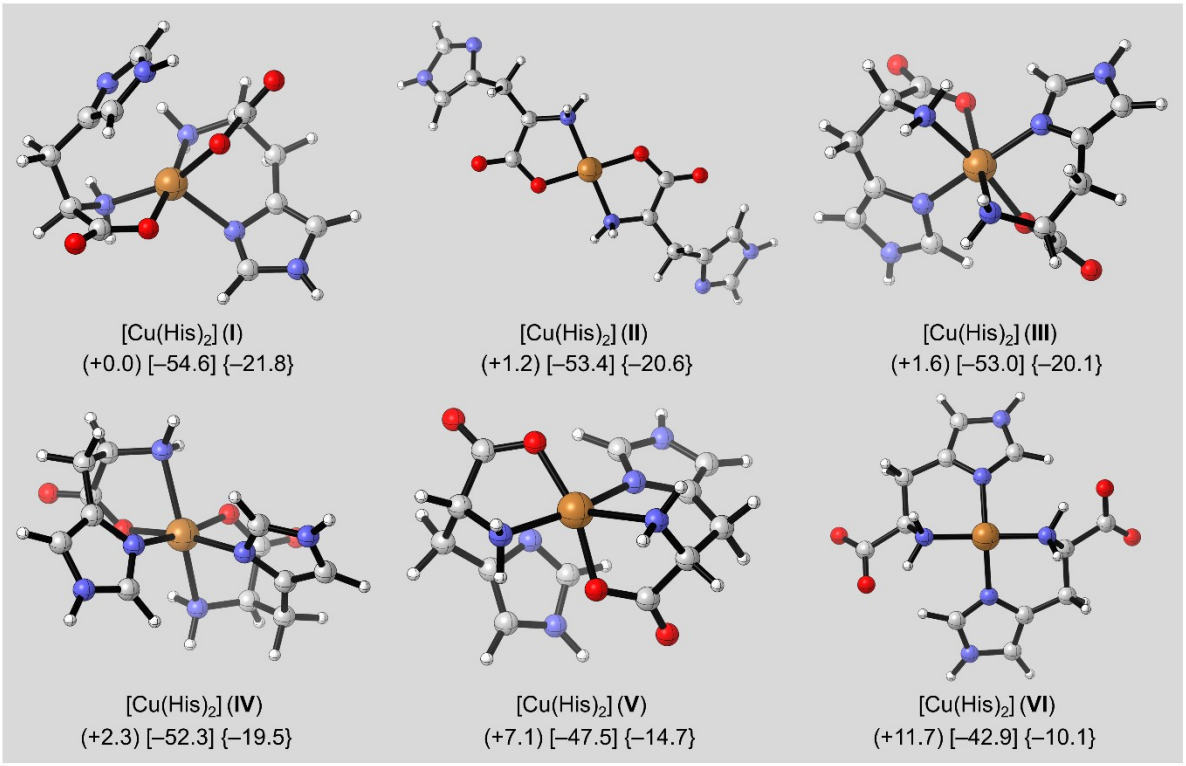

Figure S18 Free energies of all $[Cu(His)_2]$ structures investigated herein at the SMD/PBE0-D3(BJ)/bs2 level of theory. The numbers below the 3D plots are ΔG_0, ΔG_4, and ΔG_6, expressed in kcal mol^{-1}. Geometries were optimised at the PBE0-D3(BJ)/bs1 level. Gray: carbon; white: hydrogen; red: oxygen; blue: nitrogen; orange: copper.

Table S1 Calculated energy data of all species obtained in this work. Electronic energy (***E***) at the SMD/PBE0-D3(BJ)/bs2 level of theory, without zero-point energy (ZPE) correction; Corrected Gibbs free energy ($G_{298,corr}$) calculated at the PBE0-D3(BJ)/bs1 level; total Gibbs free energy (G_{298}), which incorporates the sum of ***E***, $G_{298,corr}$, and the concentration correction factor ($G_{298,conc}$) of 1.89 kcal mol^{-1}. Only the main isomers found are shown. All values are given in Hartree (Ha).

	E	$G_{298,corr}$	G_{298}
Cl^-	-460.227934	-0.015023	-460.239945
$CuCl_2$	-2560.542410	-0.024809	-2560.564207
L	-1122.718522	0.314505	-1122.401005
$CuCl_2$L	-3683.332633	0.312077	-3683.017544
Cys^{2-} (**I**)	-720.638456	0.054204	-720.581240
Cys^{2-} (**II**)	-720.636974	0.053400	-720.580562
Cys^{2-} (**III**)	-720.636175	0.054008	-720.579155
Cys^{2-} (**IV**)	-720.631263	0.052873	-720.575378
Cys^-	-721.128815	0.063518	-721.062285
Cys	-721.610403	0.075034	-721.532357
His^-	-547.940049	0.112915	-547.824122
[CuCys] (***N,S***)	-2360.771914	0.050908	-2360.717994
[CuCys] (***O,S***)	-2360.767893	0.052606	-2360.712275
[CuCys] (***N,O***)	-2360.749337	0.053764	-2360.692561
[CuCys] (***O,O***)	-2360.732741	0.050372	-2360.679357
[CuCys] (***N,S,O***)	-2360.779571	0.055085	-2360.721474
$[CuCysCl_2]^{2-}$ (***N,S***)	-3281.292531	0.049223	-3281.240296
$[CuCysCl_2]^{2-}$ (***O,S***)	-3281.264972	0.047543	-3281.214417
$[CuCysCl_2]^{2-}$ (***N,O***)	-3281.279487	0.049353	-3281.227122
$[CuCysCl_2]^{2-}$ (***O,O***)	-3281.256259	0.044938	-3281.208309
$[CuCysCl_2]^{2-}$ (***N,S,O***)	-3281.270481	0.052051	-3281.215419
$[CuHisCl_2]^-$ (**I**)	-3108.571934	0.109894	-3108.459028
$[CuHisCl_2]^-$ (**II**)	-3108.569427	0.108058	-3108.458357
$[CuHisCl_2]^-$ (**III**)	-3108.569046	0.108298	-3108.457736
$[CuHisCl_2]^-$ (**IV**)	-3108.562274	0.109195	-3108.450067
$[Cu(His)_2]$ (**I**)	-2736.077539	0.254965	-2735.819562
$[Cu(His)_2]$ (**II**)	-2736.070932	0.250252	-2735.817668
$[Cu(His)_2]$ (**III**)	-2736.075283	0.255287	-2735.816984
$[Cu(His)_2]$ (**IV**)	-2736.072545	0.253632	-2735.815901
$[Cu(His)_2]$ (**V**)	-2736.066398	0.255115	-2735.808271
$[Cu(His)_2]$ (**VI**)	-2736.061017	0.257026	-2735.800979
$[CuCysCl_2]^-$ (***N,O***)	-3281.756743	0.058209	-3281.695522
$[CuCysCl_2]^-$ (***O,O***)	-3281.742851	0.053911	-3281.685928
$[CuCysCl_2]^-$ (***N,S***)	-3281.745708	0.057398	-3281.685298
$[CuCysCl_2]^-$ (***O,S***)	-3281.739763	0.056830	-3281.679921
$[CuCysCl_2]$ (***N,S***)	-3282.203376	0.069954	-3282.130410
$[CuCysCl_2]$ (***N,O***)	-3282.196087	0.069549	-3282.123526
$[CuCysCl_2]$ (***O,S***)	-3282.184994	0.071824	-3282.110158

$[CuCysCl_2]$ (***O,O***)	-3282.180233	0.068620	-3282.108601

Table S2 Calculated ligand exchange free energy data (ΔG_2) of all neutral, anionic and dianionic $[CuCysCl_2]^{q-}$ ligands (q=0-2) obtained in this work. Equation 2.1 was adapted for the calculation of the neutral and anionic ligands. All free energy values are obtained at the SMD/PBE0-D3(BJ)/bs2 level of theory, from structures optimised at the PBE0-D3(BJ)/bs1 level. Concentration corrections are included.

	ΔG_2 (Ha)	ΔG_2 (kcal mol^{-1})
A) Cys (neutral ligand)		
$[CuCysCl_2]$ (***N,S***)	0.018486	+11.6
$[CuCysCl_2]$ (***N,O***)	0.025370	+15.9
$[CuCysCl_2]$ (***O,S***)	0.038739	+24.3
$[CuCysCl_2]$ (***O,O***)	0.040296	+25.3
B) Cys$^-$ (anionic ligand)		
$[CuCysCl_2]^-$ (***N,O***)	-0.016697	-10.5
$[CuCysCl_2]^-$ (***O,O***)	-0.007104	-4.5
$[CuCysCl_2]^-$ (***N,S***)	-0.006474	-4.1
$[CuCysCl_2]^-$ (***O,S***)	-0.001097	-0.7
C) Cys^{2-} (dianionic ligand)		
$[CuCysCl_2]^{2-}$ (***N,S***)	-0.042517	-26.7
$[CuCysCl_2]^{2-}$ (***O,S***)	-0.016637	-10.4
$[CuCysCl_2]^{2-}$ (***N,O***)	-0.029343	-18.4
$[CuCysCl_2]^{2-}$ (***O,O***)	-0.010530	-6.6
$[CuCysCl_2]^{2-}$ (***N,S,O***)	-0.017639	-11.1